

## Optimal bistable switching in nonlinear photonic crystals

Marin Soljačić,<sup>1</sup> Mihai Ibanescu,<sup>1</sup> Steven G. Johnson,<sup>1</sup> Yoel Fink,<sup>2</sup> and J. D. Joannopoulos<sup>1</sup>

<sup>1</sup>*Department of Physics, MIT, Cambridge, Massachusetts 02139*

<sup>2</sup>*Department of Material Science and Engineering, MIT, Cambridge, Massachusetts 02139*

(Received 28 May 2002; published 11 November 2002)

We present an analytical model and numerical experiments to describe optimal bistable switching in a nonlinear photonic crystal system. It is proved that only three parameters are needed to characterize a bistable switch: the resonant frequency  $\omega_{\text{res}}$ , the quality factor  $Q$ , and parameter  $\kappa$  that measures nonlinear “feedback strength.” A photonic crystal enables the device to operate in single-mode fashion, as if it were effectively one dimensional. This provides optimal control over the input and output and facilitates further large-scale optical integration.

DOI: 10.1103/PhysRevE.66.055601

PACS number(s): 42.70.Qs

A powerful principle that could be explored to implement all-optical transistors, switches, logical gates, and memory is the concept of optical bistability. In systems that display optical bistability, the outgoing intensity is a strong nonlinear function of the input intensity, and might even display a hysteresis loop. In this work, we use the flexibility offered by photonic crystals [1–3] to design a system that is effectively one dimensional (1D), although it is embedded in a higher-dimensional world. Because our system is one dimensional and single mode, it differs from previous studies [4–6] and provides optimal control over the input and output. For example, one can achieve 100% peak theoretical transmission. Moreover, the use of photonic crystals enables the system to be of a size on the order of the wavelength of light, consume only a few milliwatts of power, and have a recovery and response time smaller than 1 ps. As a consequence, the system is particularly suitable for large-scale all-optical integration. We solve the full nonlinear Maxwell’s equations numerically (with minimal physical approximations) to demonstrate optical bistability in this system. We also develop an analytical model that excellently describes the behavior of the system and is very useful in predicting and elucidating bistability phenomena.

Ideally, we would like to work with a 3D photonic crystal system. Recently, however, a 3D photonic crystal structure has been introduced that can closely emulate the photonic state frequencies and field patterns of 2D photonic crystal (PC) systems [7]. In particular, cross sections of point and line-defect modes in that structure are very similar to the profiles of the modes we describe in the present paper. We can therefore simplify our calculations without loss of generality by constructing the system in 2D. Our design is shown in Fig. 1. It resides in a square lattice 2D PC of high- $n$  dielectric rods ( $n_H = 3.5$ ) embedded in a low- $n$  dielectric material ( $n_L = 1.5$ ). The lattice spacing is denoted by  $a$ , and the radius of each rod is  $r = a/4$ . We focus our attention on transverse-magnetic (TM) modes, which have electric field parallel to the rods. To create single-mode waveguides (line defects) inside of this PC, we reduce the radius of each rod in

a line to  $r/3$ .<sup>1</sup> Further, we also create a resonant cavity (point defect) that supports a dipole-type localized resonant mode by increasing the radius of a single rod to  $5r/3$ . We connect this cavity to the outside world by placing it three unperturbed rods away from the two waveguides, one of the waveguides serving as the input port to the cavity and the other serving as the output port. The cavity couples to the two ports through tunneling processes. It is important for optimal transmission that the cavity be identically coupled to the input and output ports. We consider a physical system where the high-index material has an instantaneous Kerr nonlinearity (index change of  $n_H c \epsilon_0 n_2 |\mathbf{E}(x, y, t)|^2$ , where  $n_2$  is the Kerr coefficient). We neglect the Kerr effects in the low-index material. In order to simplify computations without sacrificing the physics, we consider only the region within the square of  $\pm 3$  rods from the cavity to be nonlinear. Essentially all of the energy of the resonant mode is within this square, so it is the only region where the nonlinearity will have a significant effect.

Consider now numerical experiments to explore the behavior of the device. Namely, we solve the full 2D nonlinear finite-difference time-domain equations [8], with perfectly matched layer boundary regions to simulate our system. The nature of these simulations is that they model Maxwell’s equations *exactly*, except for the discretization; as one increases the numerical resolution, these simulations should asymptotically reproduce what is obtained in an experiment. Most of the simulations are performed at a resolution of  $12 \times 12$  pixels per  $a \times a$ ; doubling the resolution changes the results by less than 1%. To match the waveguide modes inside the PC to the PML region, the PC waveguide is terminated with a distributed-Bragg reflector [9].

The system is designed so that it has a TM band gap of 18% between  $\omega_{\text{min}} = 0.24(2\pi c)/a$ , and  $\omega_{\text{max}} = 0.29(2\pi c)/a$ . Furthermore, the single-mode waveguide

<sup>1</sup>Note that this is just one particular way of implementing line defects in PCs; a more common way to create a line defect would be to completely remove an entire line of rods.

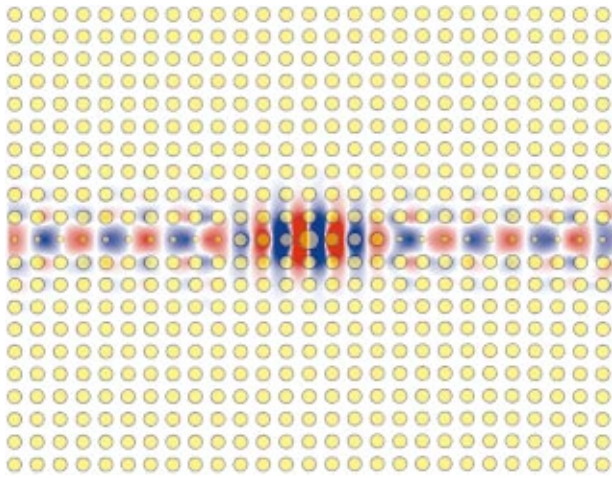


FIG. 1. (Color) Electric field for a photonic crystal bistable switch at 100% resonant linear transmission. The device consists of a resonant cavity in a square lattice of high dielectric (nonlinear) rods coupled (via tunneling effects) to two waveguides that serve as input and output ports.

created can guide all of the frequencies in the TM band gap. Finally, the cavity is designed to have a resonant frequency of  $\omega_{\text{res}} = 0.2581(2\pi c)/a$  and a Lorentzian transmission spectrum:  $T(\omega) \equiv P_{\text{out}}(\omega)/P_{\text{in}}(\omega) \approx \gamma^2/[\gamma^2 + (\omega - \omega_{\text{res}})^2]$ , where  $P_{\text{out}}$  and  $P_{\text{in}}$  are the outgoing and incoming powers, respectively, and  $\gamma$  is the width of the resonance. The quality factor of the cavity is found to be  $Q = \omega_{\text{res}}/2\gamma = 557$ .

As a first numerical experiment, we launch off-resonance pulses whose envelope is Gaussian in time, with full-width at half-maximum  $\Delta\omega/\omega_0 = 1/1595$ , into the input waveguide. The carrier frequency of the pulses is  $\omega_0 = 0.2573(2\pi c)/a$  so  $\omega_{\text{res}} - \omega_0 = 3.8\gamma$ . When the peak power of the pulses is low, the total output-pulse energy ( $E_{\text{out}} \equiv \int_{-\infty}^{\infty} dt P_{\text{out}}$ ) is only a small fraction (6.5%) of the incoming pulse energy  $E_{\text{in}}$  since we are operating off-resonance. As we increase the incoming pulse energy, the ratio  $E_{\text{out}}/E_{\text{in}}$  increases, at first slowly. However, as we approach the value of  $E_{\text{in}} = (0.57 \times 10^{-1})[(\lambda_0)^2/cn_2]^2$ , the ratio  $E_{\text{out}}/E_{\text{in}}$  grows rapidly to 0.36, after this point,  $E_{\text{out}}/E_{\text{in}}$  slowly decreases as we increase  $E_{\text{in}}$ . The dependence of  $E_{\text{out}}/E_{\text{in}}$  vs  $E_{\text{in}}$  is shown in Fig. 2.

Intuitively, as one increases the optical power, the increasing index due to the nonlinearity lowers  $\omega_{\text{res}}$  through  $\omega_0$ , causing a rise and fall in transmission. This simple picture however is modified by nonlinear feedback: as one moves into the resonance, coupling to the cavity is enhanced (positive feedback) creating a sharper on-transition and as one moves out of the resonance, the coupling is reduced (negative feedback) causing a more gradual off-transition.

Consider now a repetition of the above simulation; but with continuous-wave (CW) signals launched into the cavity instead of Gaussian pulses. There are two reasons for doing this. First, the upper branch of the expected hysteresis curve

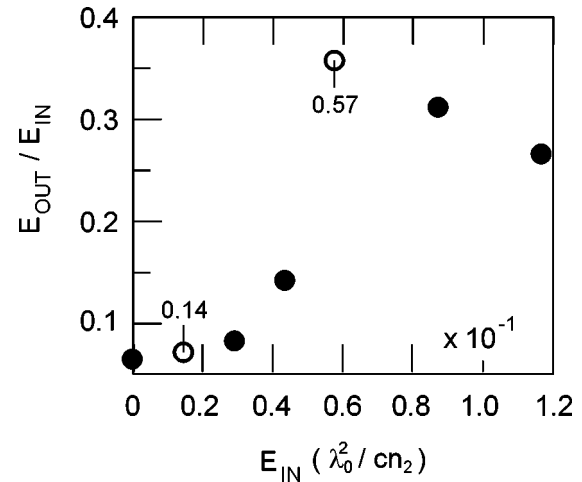


FIG. 2. Transmission of Gaussian-envelope pulses through the device of Fig. 1. As  $E_{\text{in}}$  is increased, the  $E_{\text{out}}/E_{\text{in}}$  ratio slowly grows. At a large enough  $E_{\text{in}}$ , the ratio of the outgoing and incoming pulse energies increases sharply.

is difficult to probe using only a single input pulse. Second, it is much simpler to construct an analytical theory explaining the phenomena when CW signals are used. In all cases, we find that the amplitudes of the input signals grow slowly (compared with the cavity decay time) from zero to some final CW steady-state values. Denoting by  $P_{\text{in}}^S$ ,  $P_{\text{out}}^S$  the steady-state values of  $P_{\text{in}}$  and  $P_{\text{out}}$ , respectively, we obtain the results shown by red circles in Fig. 3. For low  $P_{\text{in}}^S$ ,  $P_{\text{out}}^S$  slowly increases with increasing  $P_{\text{in}}^S$ . However, at a certain  $P_{\text{in}}^S$ ,  $P_{\text{out}}^S$  jumps discontinuously. This is precisely the desired performance, but it is not the full story.

Hysteresis loops occur quite commonly in systems that exhibit optical bistability; an upper hysteresis branch is the physical manifestation of the fact that the system “remembers” that it had a high  $P_{\text{out}}/P_{\text{in}}$  value prior to getting to the current value. To observe the upper hysteresis branch, we launch pulses that are superpositions of CW signals and

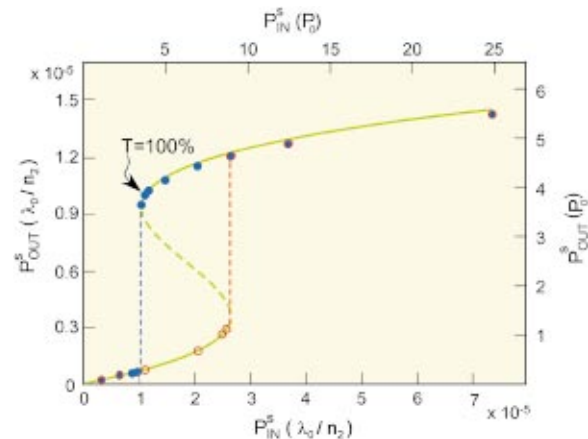


FIG. 3. (Color) Plot of  $P_{\text{out}}^S$  vs  $P_{\text{in}}^S$  for the device of Fig. 1. The red circles are obtained by launching CW signals into the device. The blue dots correspond to launching superpositions of Gaussian pulses and cw signals into the cavity in order to access the hysteresis portion of the curve. The green line is the analytical prediction, corresponding to  $\delta = 3.8$  and  $P_0 = 2.6 \times 10^{-6} \lambda_0/n_2$ .

<sup>2</sup>Here,  $\lambda_0$  is the carrier wavelength in vacuum.

Gaussian pulses (where the peak of the Gaussian pulse is significantly higher than the CW steady-state value). In this way the Gaussian pulse will “trigger” the device into a high  $P_{\text{out}}/P_{\text{in}}$  state and, as the  $P_{\text{in}}$  relaxes to its (lower) CW value, the  $P_{\text{out}}$  will eventually reach a steady-state point on the upper hysteresis branch. This is confirmed in Fig. 3 where we plot  $P_{\text{out}}^S$  as blue dots. After the CW value of  $P_{\text{in}}^S$  passes the threshold of the upper hysteresis branch, the  $P_{\text{out}}^S$  value is always on the upper hysteresis branch.

For the case of CW signals, one can achieve a precise analytical understanding of the phenomena observed. In particular, we demonstrate below that there is a single additional fundamental physical quantity associated with this cavity (in addition to  $Q$  and  $\omega_{\text{res}}$ ) that allows one to fully predict the  $P_{\text{out}}^S(P_{\text{in}}^S)$  behavior of the system. First, according to first-order perturbation theory, the field of the resonant mode will (through the Kerr effect) induce a change in the resonant frequency of the mode, given by

$$\frac{\delta\omega}{\omega_{\text{res}}} = -\frac{1}{4} \frac{\int_{\text{vol}} d^d \mathbf{r} [|\mathbf{E}(\mathbf{r}) \cdot \mathbf{E}(\mathbf{r})|^2 + 2|\mathbf{E}(\mathbf{r}) \cdot \mathbf{E}^*(\mathbf{r})|^2] n^2(\mathbf{r}) n_2(\mathbf{r}) c \varepsilon_0}{\int_{\text{vol}} d^d \mathbf{r} |\mathbf{E}(\mathbf{r})|^2 n^2(\mathbf{r})}, \quad (1)$$

where  $n(\mathbf{r})$  is the unperturbed index of refraction,  $\mathbf{E}(\mathbf{r}, t) = [\mathbf{E}(\mathbf{r}) \exp(i\omega t) + \mathbf{E}^*(\mathbf{r}) \exp(-i\omega t)]/2$  is the electric field,  $n_2(\mathbf{r})$  is the local Kerr coefficient,  $c \varepsilon_0 n_2(\mathbf{r}) n(\mathbf{r}) |\mathbf{E}(\mathbf{r})|^2 \equiv \delta n(\mathbf{r})$  is the local nonlinear index change, vol of integration is over the extent of the mode, and  $d$  is the dimensionality of our system. We now introduce a dimensionless and scale-invariant parameter  $\kappa$ , defined as

$$\kappa \equiv \left( \frac{c}{\omega_{\text{res}}} \right)^d \frac{\int_{\text{vol}} d^d \mathbf{r} [|\mathbf{E}(\mathbf{r}) \cdot \mathbf{E}(\mathbf{r})|^2 + 2|\mathbf{E}(\mathbf{r}) \cdot \mathbf{E}^*(\mathbf{r})|^2] n^2(\mathbf{r}) n_2(\mathbf{r})}{\left[ \int_{\text{vol}} d^d \mathbf{r} |\mathbf{E}(\mathbf{r})|^2 n^2(\mathbf{r}) \right]^2 n_2(\mathbf{r}) \Big|_{\text{max}}}. \quad (2)$$

As we shall see below,  $\kappa$  is a measure of the geometric nonlinear feedback efficiency of the system. We thus call  $\kappa$  the *nonlinear feedback parameter*.  $\kappa$  is determined by the degree of spatial confinement of the field in the nonlinear material; it is a very weak function of everything else.  $\kappa$  is scale invariant because of the factor  $(c/\omega_{\text{res}})^d$ , and is independent of the material  $n_2$  because of the factor  $n_2(\mathbf{r}) \Big|_{\text{max}}$  [the maximum value of  $n_2(\mathbf{r})$  anywhere]. Because the change in the field pattern of the mode due to the nonlinear effects (or due to small deviations from the operating frequency) is negligible,  $\kappa$  will also be independent of the peak amplitude. Moreover, since the spatial extent of the mode changes negligibly with a change in the  $Q$  of the cavity,  $\kappa$  is independent of  $Q$ . We found this to be true within 1% for cavities with  $Q = 557, 2190,$  and  $10\,330$  (corresponding, respectively, to 3, 4, and 5 unperturbed rods comprising the walls.) Indeed we find  $\kappa = 0.195 \pm 0.006$  across all the simulations in this work, regardless of input power,  $Q$ , and operating frequency. (For comparison, if one had a system in which all the energy of the mode were contained uniformly inside a volume  $(\lambda_0/2n_H)^3$ ,  $\kappa$  would be  $\approx 0.34$ .) Thus,  $\kappa$  is an independent design parameter. The larger the  $\kappa$ , the more efficient the system is. Moreover,  $\kappa$  facilitates system design since a single simulation is enough to determine it. One can then add rods to get the desired  $Q$ , and change the operating frequency  $\omega_0$  until one gets the desired properties.

Let us now construct an analytical model to predict the nonlinear response of a cavity in terms of only three fundamental quantities: the resonance frequency  $\omega_{\text{res}}$ , the quality factor  $Q$ , and the nonlinear feedback parameter  $\kappa$ . From Eqs. (1) and (2), we get  $\delta\omega = -(1/2)(\omega_{\text{res}}/c)^d \kappa Q c P_{\text{out}}^S n_2(\mathbf{r}) \Big|_{\text{max}}$ ; to see this note that the integral in the denominator of those equations is proportional to the energy stored in the cavity,

which is in turn proportional to  $Q P_{\text{out}}^S$ . Next, a Lorentzian resonant transmission gives  $P_{\text{out}}^S/P_{\text{in}}^S = \gamma^2 / [\gamma^2 + (\omega_0 - \delta\omega - \omega_{\text{res}})^2]$ . This expression can be simplified by defining two useful quantities:  $\delta = (\omega_{\text{res}} - \omega_0)/\gamma$ , the relative detuning of the carrier frequency from the resonance frequency, and  $P_0 \equiv 1 / [\kappa Q^2 (\omega_{\text{res}}/c)^{d-1} n_2(\mathbf{r}) \Big|_{\text{max}}]$ , a “characteristic power” of the cavity. With these definitions the relation between  $P_{\text{out}}^S$  and  $P_{\text{in}}^S$  becomes

$$\frac{P_{\text{out}}^S}{P_{\text{in}}^S} = \frac{1}{1 + (P_{\text{out}}^S/P_0 - \delta)^2}. \quad (3)$$

Thus,  $P_{\text{out}}^S(P_{\text{in}}^S)$  is now reduced to depend on only two parameters,  $P_0$  and  $\delta$ , each one of them having separate effects: a change in  $P_0$  is equivalent to a rescaling of both axes by the same factor, while the shape of the curve can only be modified by changing  $\delta$ . In general, cubic equation (3) can have either one or three real solutions for  $P_{\text{out}}^S$ , depending on the value of the detuning parameter  $\delta$ . The bistable regime corresponds to three real solutions and requires a detuning parameter  $\delta > \sqrt{3}$ . As mentioned earlier, the detuning in our simulations is  $\omega_{\text{res}} - \omega_0 = 3.8\gamma$ , which means that  $\delta = 3.8$ , which is well within the predicted bistability regime. Equation (3) is plotted in Fig. 3 as a green line for the case of  $Q = 557$  and  $\kappa = 0.195$ . It is in excellent agreement with the results from the computational experiments, predicting both the upper and lower hysteresis branches exactly. Note that the middle branch (dashed green line) is unstable in that tiny perturbations cause the solution to decay to either the upper, or lower branch [10].

From Eq. (3) one can also calculate some typical power levels for the device. For example, the input power needed for 100% transmission can be seen to be  $P_{100\%} = \delta P_0$  (corresponding to  $P_{\text{in}}^S = 3.8P_0$  in Fig. 3.) The minimum power needed for bistability is attained when  $\delta = \sqrt{3}$  in which case we obtain  $P_{b,\text{min}} = \sqrt{3}P_0 = \sqrt{3} / [\kappa Q^2 (\omega_{\text{res}}/c)^{d-1} n_2(\mathbf{r})]_{\text{max}}$ .

Since the profiles of our modes are so similar to the cross sections of the 3D modes described in Ref. [7], we can use our 2D simulations to estimate the power needed to operate a true 3D device. According to what is shown in Ref. [7], we are safe to assume that in a 3D device, the profile of the mode at different positions in the third dimension will be roughly the same as the profile of the mode in the transverse direction of the 2D system. Thus, taking the Kerr coefficient to be  $n_2 = 1.5 \times 10^{-17} \text{ m}^2/\text{W}$ , (a value achievable in many nearly instantaneous nonlinear materials), and a carrier wavelength  $\lambda_0 = 1.55 \mu\text{m}$ , gives a characteristic power of  $P_0 = 77 \text{ mW}$ , and a minimum power to observe bistability of  $P_{b,\text{min}} = 133 \text{ mW}$ .

This level of power is many orders of magnitude lower than that required by other small all-optical ultrafast switches. There are two reasons for this. First, the transverse area of the modes in the photonic crystal in question is only  $\approx (\lambda/5)^2$ ; consequently, to achieve the same-size nonlinear effects (which depend on intensity), we need much less power than in other systems that have larger transverse modal area. Second, since we are dealing with a highly confined, high- $Q$  cavity, the field inside the cavity is much larger

than the field outside the cavity; this happens because of energy accumulation in the cavity. In fact, from the expression for the characteristic power  $P_0$ , one can see that the operating power falls as  $1/Q^2$ . Building a high- $Q$  cavity that is also highly confined is very difficult in systems other than photonic crystals, so we expect high- $Q$  cavities in photonic crystals to be nearly optimal systems with respect to the power required for optical bistability. For example, a  $Q = 4000$  would be quite useful for telecommunications, and leads to the operational power of roughly 2.6 mW. Moreover, the peak  $\delta n/n$  needed to operate the device would be  $< 0.001$ , which is definitely possible with conventional instantaneous Kerr materials. Consequently, the material response and recovery time could easily be smaller than 1 ps. Potential applications for such a device include: optical logical gates, switches, optical regeneration, all-optical memory, and amplification [10].

We are especially grateful to Steve Jacobs, Torkel Engness, Ori Weisberg, and Maksim Skorobogatiy from OmniGuide Communications, Inc., for their help in developing the nonlinear finite-difference time-domain code used in these simulations. We would also like to thank Professor Shanhui Fan from Stanford University for many useful conversations. This work was supported in part by the Materials Research Science and Engineering Center program of the National Science Foundation under Grant No. DMR-9400334.

- 
- [1] E. Yablonovitch, *Phys. Rev. Lett.* **58**, 2059 (1987).  
 [2] S. John, *Phys. Rev. Lett.* **58**, 2486 (1987).  
 [3] J. D. Joannopoulos, R. D. Meade, and J. N. Winn, *Photonic Crystals: Molding the Flow of Light* (Princeton University Press, Princeton, NJ, 1995).  
 [4] S. F. Mingaleev, and Y. S. Kivshar, *J. Opt. Soc. Am. B* **19**, 2241 (2002).  
 [5] E. Centeno and D. Felbacq, *Phys. Rev. B* **62**, R7683 (2000).  
 [6] B. Xu and N. Ming, *Phys. Rev. Lett.* **71**, 3959 (1993).  
 [7] M. L. Povinelli, S. G. Johnson, S. Fan, and J. D. Joannopoulos, *Phys. Rev. B* **64**, 075313 (2001).  
 [8] For a review, see A. Taflov, *Computational Electrodynamics: The Finite-Difference Time-Domain Method* (Artech House, Norwood, MA 1995).  
 [9] A. Mekis, S. Fan, and J. D. Joannopoulos, *IEEE Microwave Guid. Wave Lett.* **9**, 502 (1999).  
 [10] B. E. A. Saleh and M. C. Teich, *Fundamentals of Photonics* (Wiley, New York, 1991).